HHS Public Access

Author manuscript

Clin Neurophysiol. Author manuscript; available in PMC 2024 September 01.

Published in final edited form as:

Clin Neurophysiol. 2023 September ; 153: 21–27. doi:10.1016/j.clinph.2023.05.013.

Decreased thalamocortical connectivity in resolved Rolandic epilepsy

Dhinakaran M. Chinappen[1,2,*], **Lauren M. Ostrowski**[1], **Elizabeth R. Spencer**[1,2], **Hunki Kwon**[1], **Mark A. Kramer**[3], **Matti S. Hämäläinen**[4,5,6], **Catherine J. Chu**[1,6,*]

[1]Massachusetts General Hospital, Department of Neurology, Boston, MA 02114, USA

[2]Graduate Program in Neuroscience, Boston University, Boston, MA 02215, USA

[3]Department of Mathematics and Statistics and Center for Systems Neuroscience, Boston University, Boston, MA 02215, USA

[4]Massachusetts General Hospital, Department of Radiology, Boston, MA 02114, USA

[5]Athinoula A, Martinos Center for Biomedical Imaging, Charlestown, MA 02129, USA

[6]Harvard Medical School, Boston, MA 02115, USA

Abstract

Objective: Median nerve somatosensory evoked fields (SEFs) conduction times reflect the integrity of neural transmission across the thalamocortical circuit. We hypothesized median nerve SEF conduction time would be abnormal in children with Rolandic epilepsy (RE).

Methods: 22 children with RE (10 active; 12 resolved) and 13 age-matched controls underwent structural and diffusion MRI and median nerve and visual stimulation during magnetoencephalography (MEG). N20 SEF responses were identified in contralateral somatosensory cortices. P100 were identified in contralateral occipital cortices as controls. Conduction times were compared between groups in linear models controlling for height. N20 conduction time was also compared to thalamic volume and Rolandic thalamocortical structural connectivity inferred using probabilistic tractography.

Results: The RE group had slower N20 conduction compared to controls (p=0.042, effect size 0.6 ms) and this difference was driven by the resolved RE group (p=0.046). There was no difference in P100 conduction time between groups (p=0.83). Ventral thalamic volume positively correlated with N20 conduction time (p=0.014).

[*]**Corresponding authors:** Dhinakaran M. Chinappen and Catherine J. Chu, Address: 100 Cambridge St., 20th floor, Boston, MA 02114, USA, dchinappen@mgh.harvard.edu; cjchu@mgh.harvard.edu.

Disclosures

None of the authors has any conflict of interest to disclose.

Ethical Publication Statement

We confirm that we have read the Journal's position on issues involved in ethical publication and affirm that this report is consistent with those guidelines.

Conclusions: Children with resolved RE have focally decreased Rolandic thalamocortical connectivity.

Significance: These results identify a persistent focal thalamocortical circuit abnormality in resolved RE and suggest that decreased Rolandic thalamocortical connectivity may support symptom resolution in this self-limited epilepsy.

Keywords

BECTS; CECTS; SeLECTS; self-limited epilepsy with centrotemporal spikes; idiopathic focal epilepsy; thalamus

1. INTRODUCTION

Rolandic epilepsy (RE, also called self-limited epilepsy with centrotemporal spikes, SeLECTS) is the most common focal developmental epileptic encephalopathy, characterized by a transient period of mild to severe cognitive symptoms and sleep-potentiated interictal spikes and seizures arising from the sensorimotor cortex (Wickens et al., 2017; Thorn et al., 2020). Rolandic epilepsy overlaps clinically with more severe epilepsy aphasia syndromes, and sparse cases have been linked to a monogenic gene mutation (Carvill et al., 2013). Electrographic features are highly penetrant between first-degree relatives, but disease symptoms can also be discordant between monozygotic twins suggesting a complex interplay between genes, environment, and development may contribute to symptom expression in RE (Bray et al., 1964; Bray et al., 1965; Vadlamudi et al., 2006). RE symptoms and electrophysiology lie on a spectrum with continuous spike-wave during slow wave sleep, Landau-Kleffner syndrome, and centrotemporal spikes and sharp waves without epilepsy (Lemke et al., 2017). Most children with RE have cognitive deficits detected on formal testing during the active phase of the disease (Wickens et al., 2017). Seizures and cognitive symptoms are both self-limited (Ross et al., 2020).

Electrophysiological and structural evidence implicate focal dysfunction of the Rolandic thalamocortical circuits in RE. Children with RE have focally abnormal white matter microstructure near the sensorimotor cortex (Ostrowski et al., 2019; Ciumas et al., 2014; Kim et al., 2013). Sleep spindles, which are generated in the reticular nucleus of the thalamus and entrained in thalamocortical circuits, are focally decreased in the sensorimotor cortex in children with RE during the active phase of the disease (Beenhakker et al., 2009; Kramer et al., 2021). Clinical symptoms -- seizures and cognitive symptoms – and electrographic features – epileptiform spikes and sleep spindle deficits – resolve in disease resolution (Kramer et al., 2021; Ross et al., 2020; Xie et al., 2018). Direct measures of thalamocortical white matter connectivity reveal that children with RE have abnormal structural and functional thalamocortical connectivity to the Rolandic cortex (Kwon et al., 2022), and an aberrant developmental trajectory of thalamocortical structural connectivity to the sensorimotor cortex persists beyond disease resolution (Thorn et al., 2020). Taken together, these findings demonstrate that alterations in thalamocortical connectivity persist beyond symptoms, potentially providing compensatory mechanisms that support symptom resolution.

Somatosensory evoked magnetic fields (SEFs) are summated neural responses to peripheral nerve sensory stimulation measured in the Rolandic cortex. In the case of median nerve somatosensory stimulation, neural activity arrives at the primary somatosensory cortex after transmission along peripheral nerves, dorsal medial lemniscus, and thalamocortical white matter as a dominant surface-negative signal (*e.g.*, N20) approximately 20 ms after stimulation. This evoked potential thus provides a direct assay of integrity of the Rolandic thalamocortical circuit. In contrast, visual evoked fields (VEFs) are summated neural responses to visual stimulation measured in the primary visual cortex. Neural activity arrives at the primary visual cortex after transmission from the retina, along the optic nerves and thalamocortical optic tracts as a dominant positive signal (*e.g.*, P100) approximately 100 ms after stimulation. Cortical visual evoked potentials are sensitive to subtle structural deficits along the visual pathway but are not expected to be disrupted by a disease that affects focal thalamocortical Rolandic circuits (Toosy et al., 2014).

Given converging evidence for Rolandic thalamocortical circuit dysfunction in RE, we hypothesized that median nerve SEF conduction time would be abnormal in children with RE compared to controls, reflecting aberrant functional and structural connectivity of the thalamocortical sensorimotor circuit. We further hypothesized that conduction time along the visual pathway would be similar in children with RE and controls, confirming that the thalamocortical dysfunction in RE is focal to the sensorimotor circuit. After identifying a difference in N20 conduction time, we explored the relationships between N20 conduction time and thalamic volume, ventral nucleus volume, and white matter connectivity to help localize the anatomical source of this dysfunction. Identification of focally impaired thalamocortical conduction time to the Rolandic cortex provides a novel biomarker for RE, helps localize the anatomical disruption, and provides further insight into the pathophysiology of symptoms and resolution in this common childhood disease.

2. METHODS

2.1 Subjects

Children 4–15 years of age who received a clinical diagnosis of RE by a child neurologist following 1989 International League Against Epilepsy criteria, confirmed to have a history of focal motor or generalized seizures, and an EEG showing sleep-activated centrotemporal spikes were eligible for this prospective study (International League Against Epilepsy (ILEA), 2017; ILAE, 2014). Control subjects without a history of seizure or known neurologic disorder were also recruited (n=13). RE and control subjects with a history of unrelated neurologic disease were excluded, although children with attention disorders and mild learning difficulties consistent with known RE comorbidities were included (Wickens et al., 2017). Children with RE were grouped into two categories of seizure risk: Active, defined as having had a seizure within 12 months (n=10); and Resolved, defined as being seizure free for >12 months (n=12) because most children who have been seizure free for 12 months have entered terminal remission (Ross et al., 2020). Two subjects who were initially enrolled during active disease returned after disease resolution and were included in the Resolved group.

Subject age, sex, current medications, and date of last seizure were collected at the time of visit. Subject height on the visit date was extrapolated from the subjects' individualized growth curve available from the electronic medical record (n=29, Center for Disease Control and Prevention, 2017) or from an estimate of the height provided by the child's guardian on the visit date (n=6). Subjects and their guardians gave age-appropriate informed consent according to standards reviewed by the Institutional Review Board at Massachusetts General Hospital.

2.2 Magnetoencephalogram (MEG) acquisition and processing

MEG data were recorded with a 306-sensor system at 2,035 Hz sampling rate (Elekta-Neuromag, 204 planar gradiometers and 102 magnetometers) inside a magnetically shielded room. For each recording session, the head position was recorded approximately every four minutes and deemed satisfactory based on reasonable distance values of the head and the MEG helmet.

During MEG acquisition, left and right median nerve evoked fields were collected at random median nerve inter-stimulation intervals ranging from 100 to 140 ms over a period of approximately four minutes. Subjects were instructed to stay awake and monitored via live video feed. For these data, the minimum necessary stimulation amplitude required to trigger a visibly confirmed thenar contraction was used. Following median nerve stimulation, visual evoked field data were collected during the same visit. For this, subjects were instructed to keep their eyes open and affixed to a plus sign projected on a screen in the middle of their visual field while flashing checkered patterns appeared on the screen, randomly switching across four quadrants corresponding to the right and left upper and lower visual fields with interstimulation intervals ranging from 333–525 ms.

2.3 Magnetic Resonance Imaging (MRI) acquisition

All subjects underwent structural and diffusion MRI recording as close to the day of MEG acquisition as possible (median 0.0 days between MEG and MRI, range: −22.0 to 36.0 days). All images were visually inspected by a neuroradiologist to confirm no gross structural abnormalities. All images were acquired in the same Siemens 3.0 T MRI with a 64-channel head coil at the Martinos Center for Biomedical Imaging and included: 1) T1 MultiEcho Magnetization Prepared RApid Gradient Echo (MEMPRAGE) images (176 slices, 1.0 mm slice thickness, 1.0×1.0×1.0 mm^3 voxel size, repetition time (TR): 2,530ms, inversion time (TI): 1,100ms, flip angle: 7°) with 4 different Echo Times (TE), 1.69 ms, 3.55 ms, 5.41 ms and 7.27 ms; 2) T2 Fluid Attenuated Inversion Recovery (FLAIR) (192 slices, 0.9×0.9×0.9 mm^3 voxel size, 5,000 ms TR, 1,800 ms TI, and TE 7 ms; 3) Diffusion Weighted Imaging (DWI) (64 diffusion-encoding directions, 82 ms TE, 8,080 ms TR, flip angle:90°, voxel size=2.0×2.0×2.0 mm^3, diffusion sensitivity of b=2,000 s/mm^2, number of slices=74, no skip).

2.4 Magnetic Source Imaging of SEFs and VEFs

Averaged evoked fields were detected and measured in source space. Using FreeSurfer, each participant's cortical surface was tessellated using a combination of T1 and T2-FLAIR images when available (n=31), or only the T1 images (n=2) otherwise, and decimated to

10,242 dipoles per hemisphere, corresponding to approximately 5 mm spacing between adjacent source locations (Fischl et al., 1999; Hämäläinen et al., 1987). To compute the MEG forward solution, a three-compartment boundary-element model was employed following the assumed geometrical intracranial space (FreeSurfer, 2021). Inner and outer skull and inner skin triangulations were generated using a watershed algorithm applied onto the T1 images of each participant. Minimum-norm estimate (MNE) software was applied to estimate cortical current distribution, assuming orientation of the source to be fixed perpendicular to the cortical mesh (Mamashli et al., 2017).

After acquisition, in off-line analysis, channels contaminated with artifact were identified and not considered during analysis. The noise covariance matrix was estimated from each MEG recording and the cortical generators then estimated using anatomically constrained dynamic statistical parametric mapping (dSPM). Data were filtered between 0.1 Hz and 500 Hz for somatosensory evoked responses and 1.5 Hz and 70 Hz for visually evoked responses. The data were then epoched into single trials beginning 200 ms prior to stimulus onset and ending 500 ms after stimulus onset. Epochs were rejected if the peak-to-peak amplitude during the epoch exceeded 2,000 fT/cm and 10,000 fT in any of the gradiometer or magnetometer channels, respectively. Averaged trials were subsequently analyzed from 20 ms prior to stimulus onset to 100 ms after stimulus onset for SEF, and from 20 ms prior to stimulus to 200 ms after stimuls onset for VEF.

The averaged median nerve N20 evoked potentials were contralaterally detected in the somatosensory cortex by identifying the distinct N20-P35 shape (Figure 1). Following the identification of the first clear N20 signal, the localization and tangential orientation of each dipole in the hand region of the somatosensory cortex was visually confirmed for accuracy. Subjects without an identifiable N20 evoked potential in the somatosensory cortex were excluded. For each subject, the vertex with the largest amplitude at the N20 peak was selected and the conduction time recorded contralaterally. The visual evoked potentials were detected in the occipital cortex by identifying the P100 signal. The localization and orientation of each dipole was visually confirmed to be adjacent to the pericalcarine fissure, inverted and contralateral to the corresponding visual field stimuli. Subjects without an identifiable P100 evoked potential in the visual cortex were excluded. The vertex with the largest amplitude at the P100 peak was selected and the conduction time recorded for each subject. Upper and lower quadrant results were averaged for a single measure per hemisphere.

2.5 Posthoc Analyses:

2.5.1 Thalamic volume and cortical surface measurements.—

Intracranial anatomical landmarks along the three-neuron pathway that median nerve evoked fields traverse from the wrist to the cortex were analyzed. This pathway includes synapses in the ipsilateral dorsal root ganglion and the contralateral ventral posterolateral nucleus of the thalamus. Thalamic volume estimates were performed on the T1-MEMPRAGE volumes using thalamic segmentations tools in FreeSurfer 7.1.1 (FreeSurfer, 2021; Iglesias et al., 2018). The combination of T1-MEMPRAGE and T2-FLAIR volumes were used, when available, to estimate the entire thalamic volume and regional thalamic volumes (anterior,

lateral, ventral, intralaminar and posterior) (Iglesias et al., 2018). Two subjects did not complete MRI (n=33 available for analysis). Two subjects had only T1-MEMPRAGE available.

2.5.2 Probabilistic Tractography.—From the thalamus, median nerve sensory evoked fields travel through the corona radiata white matter to the sensory cortex. To evaluate the thalamocortical structural connectivity of this circuit, probabilistic tractography was performed on available MR diffusion data (n=33).

To evaluate the Rolandic sensorimotor thalamocortical white matter, we computed the structural connectivity to the postcentral gyrus target region of interest (ROI) from two seed ROIs: a) the entire ipsilateral thalamus; and b) the ventral region of the ipsilateral thalamus. We applied ball-and-stick model-based probabilistic diffusion tensor tracking (Probtrackx2 through Functional Magnetic Resonance Imaging of the Brain (FMRIB) Software Library (FSL) 5.0.4 / FMRIB Diffusion Toolbox (FDT) (Behrens et al., 2003). The Desikan-Killiany atlas was used to segment the postcentral gyrus (Desikan et al., 2006).

BedpostX (Bayesian Estimation of Diffusion Parameters Obtained using Sampling Techniques for modeling Crossing Fibers) was used to estimate the principal diffusion direction per voxel. 500 streamlines per seed ROI voxel were sampled using Probtrackx2 with a 0.2 curvature threshold with distance correction on. A step length of 0.5 mm was used for each streamline with a maximum of 2000 steps per streamline. Streamlines were terminated when they reached the target ROI or they met the rejection criteria by each hemisphere. Loop checks were performed to prevent streamlines from looping back on themselves, and a subsidiary fiber volume threshold of 0.01 of the parent fiber volume was applied to exclude negligible volumes. Using the number of streamlines launched from the seed ROI and the number of voxels in the target ROI a Connectivity Index (CI) was calculated (Chu et al., 2015). The CI was then normalized by the volume (number of voxels) of the seed ROI. Appropriate tracts were confirmed with visual analysis.

2.6 Statistical analyses

To detect a difference in the distributions of SEF conduction times between children with RE and controls, we estimated a linear mixed effects model with group as predictor and a random subject specific intercept to account for two observations per subject (left and right SEF conduction time). Height was included as a covariate. We note that height and age are collinear and because height is expected to directly impact SEF measures, we included height instead of age as a covariate in the models.

To evaluate whether duration of epilepsy remission (duration seizure free), thalamic volume, or Rolandic thalamocortical structural connectivity predicted SEF conduction time, we estimated mixed effects models of a similar form; in separate models, we included each of these variables as a predictor, a random subject specific intercept, and height as a covariate.

To test if conduction times in the active and remission groups differed from the control subjects, we estimated linear mixed effects models with conduction time as the dependent

variable, group and height as independent variables, and a random subject-specific intercept to account for two observations per subject (left and right hemisphere SEF conduction time).

Equivalent control tests were done using VEF conduction time, group, and LGN volume.

3. RESULTS

3.1 Participant information

For SEF, 22 children with RE (mean age 11.9 years, range: 8.0–16.9 years, 3F; active RE: mean age 11.0 years, range: 9.0–14.7 years; resolved RE: mean age 12.7 years, range: 8.0–16.9) were included, of whom 8 were on anti-seizure medication (ASM). Thirteen control children (mean age 11.9 years, range 8.0–15.1 years, 7F) were included. For VEF, 22 children with RE (mean age 11.8 years, range: 9.0–16.9 years, 4F; active RE: mean age 10.5 years, range: 9.0–14.6 years; resolved RE: mean age 13.4 years, range: 10.4–16.9) were included, of whom 7 were on anti-seizure medication (ASM). Fourteen control children (mean age 12.5 years, range 9.0–15.1 years, 8F) were included. Subject characteristics are provided in Table 1.

3.2 Children with resolved RE have delayed median nerve sensory conduction time

Children with RE have delayed median nerve SEF conduction time compared to controls ($p=0.042$; effect size 0.6 ms, 95% CI [0.021, 1.201], average conduction time of RE group: 21.3 ± 1.6 ms, average conduction time of controls: 20.4 ± 1.0 ms, Figure 2A). Separating RE subjects into active or remission groups, only the SEF conduction time in the remission group differed from controls ($p=0.046$, effect size 0.7 ms, 95% CI [0.0, 1.4]; active group $p=0.48$, effect size 0.5 ms, 95% CI [−0.2, 1.2]).

3.3 No difference in VEF conduction between RE and Controls

There was no evidence of a difference in visual field P100 conduction time to the occipital cortex between RE and controls ($p=0.83$, Figure 2B). Taken together, these results identify a focal conduction delay along the Rolandic thalamocortical white matter circuit in children with resolved RE.

3.5 Ventral thalamic volume predicts SEF conduction time

We found no evidence that thalamic volume predicts SEF conduction time ($p=0.11$, effect size 0.0003 ms/mm^3, 95% CI [−0.0001, 0.0007]). However, the ventral thalamic region, through which the median nerve stimulus travels, was larger in RE compared to controls ($p=0.037$, effect size 239 mm^3, 95% CI [15, 462] mm^3, Figure 3A) and had a positive relationship with conduction time ($p=0.023$, effect size 0.0008 ms/mm^3, 95% CI [0.0001, 0.0015] ms/mm^3, Figure 3B).

3.6 Thalamocortical white matter structural connectivity does not predict SEF conduction time

To evaluate whether white matter structural connectivity predicted SEF conduction time, we used probabilistic tractography to compute the CI between somatosensory cortex and the

whole thalamus, and between somatosensory cortex and the ventral thalamus (Table 2). We found no evidence of a relationship between either CI and SEF conduction time ($p>0.3$).

DISCUSSION

In this prospective cross-sectional study, we found evidence for a conduction delay in the median nerve somatosensory evoked fields in children with resolved RE compared to control subjects. We found no evidence for a conduction abnormality in visual evoked potentials between children with RE and control subjects. Taken together, these data demonstrate an emergent abnormality in the Rolandic thalamocortical circuit in RE and suggest that focally decreased Rolandic thalamocortical connectivity may support symptom resolution in this transient focal epilepsy.

Median nerve sensory responses travel along a three-neuron pathway where the terminal neuron lies in the VPL nucleus and projects to the sensory Rolandic cortex through the corona radiata. The ventral thalamus further includes the VL thalamic nucleus which regulates sensory integration for motor control and projects to the supplementary motor regions, the VA nucleus which has projections to premotor cortex, and the VM nucleus which has projections to the somatosensory cortex and limbic structures. Investigation of this intracranial portion of the pathway revealed that the volume of the contralateral ventral thalamus positively correlated with conduction time in RE. We have previously reported abnormal Rolandic white matter structural connectivity in RE in disease resolution (Kwon et al., 2022). Increased structural connectivity would typically reflect increased myelinated fibers and support faster conduction time. Here, however, we found delayed conduction time in resolved RE. Further, conduction time correlated with ventral thalamic volume, which were larger in children with RE. Notably, prior work that has identified that children with smaller thalamic volumes and abnormal thalamocortical metabolic connectivity are at increased risk of sleep-potentiated epileptic encephalopathies (Fernández et al., 2017; Moeller et al., 2014; Agarwal et al., 2016). Thus, the positive relationship between ventral thalamic size and SEF conduction time may reflect a compensatory strategy to help inhibit the abnormal activity in this thalamocortical circuit (Li et al., 2021). Thus, the increased conduction time we see here in resolved RE may potentially reflect increased inhibitory processing at the level of the thalamus. Future mechanistic work is required to better understand this relationship.

We found that children with RE have a focal conduction delay in median nerve somatosensory evoked responses. These data suggest that the functional integrity of the thalamocortical sensorimotor circuit is abnormal in RE, and that a decrease in thalamocortical conduction may be a feature of disease resolution. Conduction time delays correlates with increased thalamic volume, implicating this node of the circuit in compensatory responses that may support symptom resolution.

Acknowledgments

This work was supported by grants NIH NINDS K23NS092923 and R01NS115868. The authors would like to thank Dan Y. Song, Wenting Xie, Emily L. Thorn, McKenna Parnes, Erin E. Ross, Sally M. Stoyell and Grace Xiao for participating in data collection. Gratitude also goes to the MEG Core team at MGH.

REFERENCES

Agarwal R, Kumar A, Tiwari VN, Chugani H. Thalamic abnormalities in children with continuous spike-wave during slow-wave sleep: An F-18-fluorodeoxyglucose positron emission tomography perspective. Epilepsia. 2016;57(2):263–71. doi: 10.1111/epi.13278. Epub 2015 Dec 24. PMID: 26697846. [PubMed: 26697846]

Behrens TE, Woolrich MW, Jenkinson M, Johansen-Berg H, Nunes RG, Clare S et al. Characterization and propagation of uncertainty in diffusion-weighted MR imaging. Magn Reson Med. 2003;50(5):1077–88. doi: 10.1002/mrm.10609. PMID: 14587019. [PubMed: 14587019]

Bechtold B. Violin Plots for Matlab, 2016. Github Project: https://github.com/bastibe/Violinplot-Matlab, doi: 10.5281/zenodo.4559847

Bray PF, Wiser WC. Evidence for a Genetic Etiology of Temporal-Central Abnormalities in Focal Epilepsy. N Engl J Med. 1964;271:926–33. doi: 10.1056/NEJM196410292711803. PMID: 14197414. [PubMed: 14197414]

Beenhakker MP, Huguenard JR. Neurons that fire together also conspire together: is normal sleep circuitry hijacked to generate epilepsy? Neuron. 2009;62(5):612–32. doi: 10.1016/j.neuron.2009.05.015. [PubMed: 19524522]

Bray PF, Wiser WC. Hereditary Characteristics of Familial Temporal-Central Focal Epilepsy. Pediatrics. Pediatrics. 1965;36:207–11. [PubMed: 14320029]

Carvill GL, Regan BM, Yendle SC, O'Roak BJ, Lozovaya N, Bruneau N et al. GRIN2A mutations cause epilepsy-aphasia spectrum disorders. Nat Genet. 2013;45(9):1073–6. doi: 10.1038/ng.2727. [PubMed: 23933818]

Centers for Disease Control and Prevention (CDC). Growth charts - Clinical growth charts. Last reviewed 2017. https://www.cdc.gov/growthcharts/clinical_charts.htm

Chu CJ, Tanaka N, Diaz J, Edlow BL, Wu O, Hämäläinen M et al. EEG functional connectivity is partially predicted by underlying white matter connectivity. Neuroimage. 2015;108:23–33. doi: 10.1016/j.neuroimage.2014.12.033. [PubMed: 25534110]

Desikan RS, Ségonne F, Fischl B, Quinn BT, Dickerson BC, Blacker D et al. An automated labeling system for subdividing the human cerebral cortex on MRI scans into gyral based regions of interest. Neuroimage. 2006;31(3):968–80. doi: 10.1016/j.neuroimage.2006.01.021. [PubMed: 16530430]

Dale AM, Sereno MI. Improved Localizadon of Cortical Activity by Combining EEG and MEG with MRI Cortical Surface Reconstruction: A Linear Approach. J Cogn Neurosci. 1993;5(2):162–76. doi: 10.1162/jocn.1993.5.2.162. [PubMed: 23972151]

Fischl B, Sereno MI, Dale AM. Cortical surface-based analysis. II: Inflation, flattening, and a surface-based coordinate system. Neuroimage. 1999;9(2):195–207. doi: 10.1006/nimg.1998.0396. [PubMed: 9931269]

Fisher RS, Acevedo C, Arzimanoglou A, Bogacz A, Cross JH, Elger CE. ILAE official report: a practical clinical definition of epilepsy. Epilepsia. 2014;55(4):475–82. doi: 10.1111/epi.12550. [PubMed: 24730690]

FreeSurfer. Available from: https://surfer.nmr.mgh.harvard.edu/. Laboratory for Computational Neuroimaging, Martinos Center for Biomedical Imaging, 2021.

Hämäläinen MS, Sarvas J. Feasibility of the homogeneous head model in the interpretation of neuromagnetic fields. Phys Med Biol. 1987;32(1):91–7. doi: 10.1088/0031-9155/32/1/014. PMID: 3823145. [PubMed: 3823145]

Hyllienmark L, Ludvigsson J, Brismar T. Normal values of nerve conduction in children and adolescents. Electroencephalogr Clin Neurophysiol. 1995;97(5):208–14. doi: 10.1016/0924-980X(95)00092-5. [PubMed: 7489681]

Iglesias JE, Insausti R, Lerma-Usabiaga G, Bocchetta M, Van Leemput K, Greve DN et al. A probabilistic atlas of the human thalamic nuclei combining ex vivo MRI and histology. Neuroimage. 2018;183:314–326. doi: 10.1016/j.neuroimage.2018.08.012. [PubMed: 30121337]

Kim SE, Lee JH, Chung HK, Lim SM, Lee HW. Alterations in white matter microstructures and cognitive dysfunctions in benign childhood epilepsy with centrotemporal spikes. Eur J Neurol. 2014;21(5):708–17. doi: 10.1111/ene.12301. [PubMed: 24330132]

Kramer MA, Stoyell SM, Chinappen D, Ostrowski LM, Spencer ER, Morgan AK et al. Focal Sleep Spindle Deficits Reveal Focal Thalamocortical Dysfunction and Predict Cognitive Deficits in Sleep Activated Developmental Epilepsy. J Neurosci. 2021;41(8):1816–1829. doi: 10.1523/JNEUROSCI.2009-20.2020. [PubMed: 33468567]

Kwon H, Chinappen DM, Huang JF, Berja ED, Walsh KG, Shi W et al. Transient, developmental functional and structural connectivity abnormalities in the thalamocortical motor network in Rolandic epilepsy. Neuroimage Clin. 2022;35:103102. doi: 10.1016/j.nicl.2022.103102.

Lee YJ, Hwang SK, Kwon S. The Clinical Spectrum of Benign Epilepsy with Centro-Temporal Spikes: a Challenge in Categorization and Predictability. J Epilepsy Res. 2017;7(1):1–6. doi: 10.14581/jer.17001. [PubMed: 28775948]

Lemke JR, Lal D, Reinthaler EM, Steiner I, Nothnagel M, Alber M. Mutations in GRIN2A cause idiopathic focal epilepsy with rolandic spikes. Nat Genet. 2013;45(9):1067–72. doi: 10.1038/ng.2728. [PubMed: 23933819]

Li Q, Westover MB, Zhang R, Chu CJ. Computational Evidence for a Competitive Thalamocortical Model of Spikes and Spindle Activity in Rolandic Epilepsy. Front Comput Neurosci. 2021;15:680549. doi: 10.3389/fncom.2021.680549.

Mamashli F, Khan S, Bharadwaj H, Michmizos K, Ganesan S, Garel KA et al. Auditory processing in noise is associated with complex patterns of disrupted functional connectivity in autism spectrum disorder. Autism Res. 2017;10(4):631–647. doi: 10.1002/aur.1714. [PubMed: 27910247]

McGinnity CJ, Smith AB, Yaakub SN, Weidenbach Gerbase S, Gammerman A, Tyson AL. Decreased functional connectivity within a language subnetwork in benign epilepsy with centrotemporal spikes. Epilepsia Open. 2017;2(2):214–225. doi: 10.1002/epi4.12051. [PubMed: 29588950]

Moeller F, Moehring J, Ick I, Steinmann E, Wolff S, Jansen O et al. EEG-fMRI in atypical benign partial epilepsy. Epilepsia. 2013;54(8):e103–8. doi: 10.1111/epi.12243. [PubMed: 23758518]

Ostrowski LM, Song DY, Thorn EL, Ross EE, Stoyell SM, Chinappen DM et al. Dysmature superficial white matter microstructure in developmental focal epilepsy. Brain Commun. 2019;1(1):fcz002. doi: 10.1093/braincomms/fcz002.

Öztürk Z, Karalok ZS, Günes A. Reduced thalamic volume is strongly associated with electrical status epilepticus in sleep. Acta Neurol Belg. 2021;121(1):211–217. doi: 10.1007/s13760-019-01202-7. [PubMed: 31456121]

Proposal for revised classification of epilepsies and epileptic syndromes. Commission on Classification and Terminology of the International League Against Epilepsy. Epilepsia. 1989;30(4):389–99. doi: 10.1111/j.1528-1157.1989.tb05316.x. [PubMed: 2502382]

Ross EE, Stoyell SM, Kramer MA, Berg AT, Chu CJ. The natural history of seizures and neuropsychiatric symptoms in childhood epilepsy with centrotemporal spikes (CECTS). Epilepsy Behav. 2020;103:106437. doi: 10.1016/j.yebeh.2019.07.038.

Spencer ER, Chinappen D, Emerton BC, Morgan AK, Hämäläinen MS, Manoach DS et al. Source EEG reveals that Rolandic epilepsy is a regional epileptic encephalopathy. Neuroimage Clin. 2022;33:102956. doi: 10.1016/j.nicl.2022.102956.

Stetson DS, Albers JW, Silverstein BA, Wolfe RA. Effects of age, sex, and anthropometric factors on nerve conduction measures. Muscle Nerve. 1992;15(10):1095–104. doi: 10.1002/mus.880151007. [PubMed: 1406766]

Stetson DS, Albers JW, Silverstein BA, Wolfe RA. Effects of age, sex, and anthropometric factors on nerve conduction measures. Muscle Nerve. 1992;15(10):1095–104. doi: 10.1002/mus.880151007. [PubMed: 1406766]

Thorn EL, Ostrowski LM, Chinappen DM, Jing J, Westover MB, Stufflebeam SM et al. Persistent abnormalities in Rolandic thalamocortical white matter circuits in childhood epilepsy with centrotemporal spikes. Epilepsia. 2020;61(11):2500–2508. doi: 10.1111/epi.16681. [PubMed: 32944938]

Vadlamudi L, Kjeldsen MJ, Corey LA, Solaas MH, Friis ML, Pellock JM et al. Analyzing the etiology of benign rolandic epilepsy: a multicenter twin collaboration. Epilepsia. 2006;47(3):550–5. doi: 10.1111/j.1528-1167.2006.00466.x. [PubMed: 16529620]

Toosy AT, Mason DF, Miller DH. Optic neuritis. Lancet Neurol. 2014;13(1):83–99. doi: 10.1016/S14744422(13)70259-X. [PubMed: 24331795]

Wang P, Li Y, Sun Y, Sun J, Niu K, Zhang K et al. Altered functional connectivity in newly diagnosed benign epilepsy with unilateral or bilateral centrotemporal spikes: A multi-frequency MEG study. Epilepsy Behav. 2021;124:108276. doi: 10.1016/j.yebeh.2021.108276.

Wickens S, Bowden SC, D'Souza W. Cognitive functioning in children with self-limited epilepsy with centrotemporal spikes: A systematic review and meta-analysis. Epilepsia. 2017;58(10):1673–1685. doi: 10.1111/epi.13865. [PubMed: 28801973]

Wu Y, Ji GJ, Zang YF, Liao W, Jin Z, Liu YL. Local Activity and Causal Connectivity in Children with Benign Epilepsy with Centrotemporal Spikes. PLoS One. 2015;10(7):e0134361. doi: 10.1371/journal.pone.0134361.

Xie W, Ross EE, Kramer MA, Eden UT, Chu CJ. Timing matters: Impact of anticonvulsant drug treatment and spikes on seizure risk in benign epilepsy with centrotemporal spikes. Epilepsia Open. 2018;3(3):409–417. doi: 10.1002/epi4.12248. [PubMed: 30187012]

Highlights

- Children with resolved Rolandic epilepsy have increased median nerve somatosensory conduction time compared to controls.
- Ventral thalamic volume positively correlated with N20 conduction time.
- Focally decreased Rolandic thalamocortical connectivity may support symptom resolution in Rolandic epilepsy.

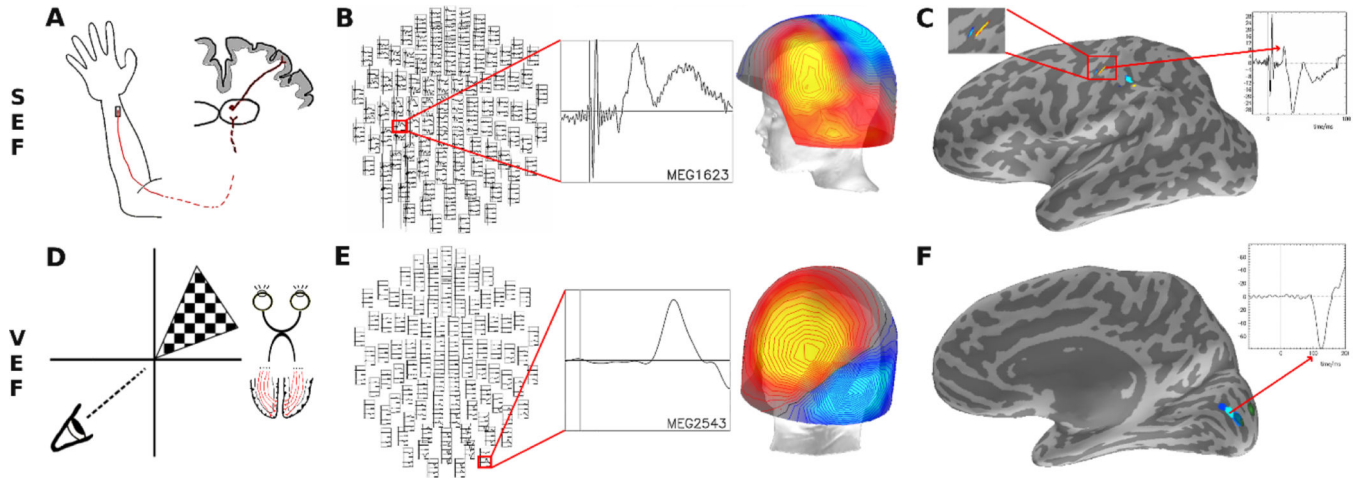

Figure 1: Experimental set up and processing.

A) For somatosensory evoked field (SEF) testing, the distal median nerve was stimulated, resulting in an evoked response that synapses in the ventroposteriolateral thalamus and then arrives as an N20 signal in the sensory cortex. B) Magnetoencephalogram (MEG) cortical recordings were averaged across trials in each hemisphere and visually inspected for a N20 dipole in sensor space. C) The peak N20 response was confirmed to localize to the hand representation area of the contralateral primary sensory cortex, and the N20 conduction time was measured as the time of the peak of the N20 amplitude deflection in source space. D) For visual evoked field (VEF) testing, checkered visual stimuli were displayed randomly in the four quadrants, resulting in an evoked response that synapses in the lateral geniculate nucleus of the thalamus and then arrives as a P100 signal in occipital cortex. E) MEG cortical recordings were averaged across trials in each hemisphere and visually inspected for a P100 dipole in sensor space. F) The peak P100 response was confirmed to localize in the contralateral pericalcarine cortex in source space and the P100 conduction time was measured as the time of the peak of the negative P100 amplitude deflection.

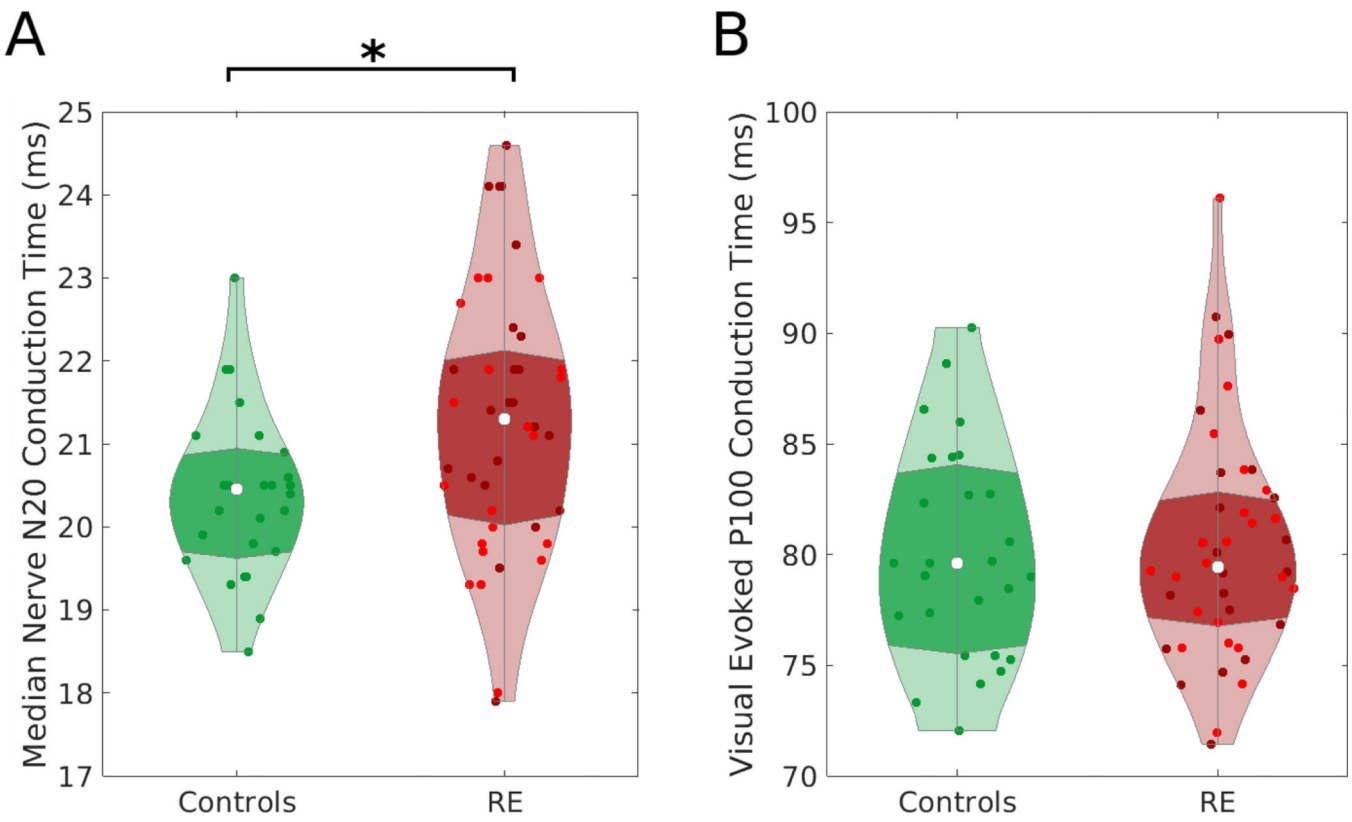

Figure 2. Somatosensory Evoked Fields (SEF), but not Visual Evoked Fields (VEF), conduction times differ in children with Rolandic epilepsy and controls.

A) Children with Rolandic Epilepsy (RE) have delayed SEF median nerve N20 conduction time compared to controls (p=0.042) B) There is no evidence of a difference in VEF P100 conduction times across groups (p=0.8). Points indicate individual hemisphere measurements. For RE, bright red indicates the active RE and darker red indicates remission RE. Violin plots (Bechtold, 2016) indicate the density of conduction time values, the violin width represents the number of points at each value, the white represents the median value, and the darker shading indicates the interquartile range.

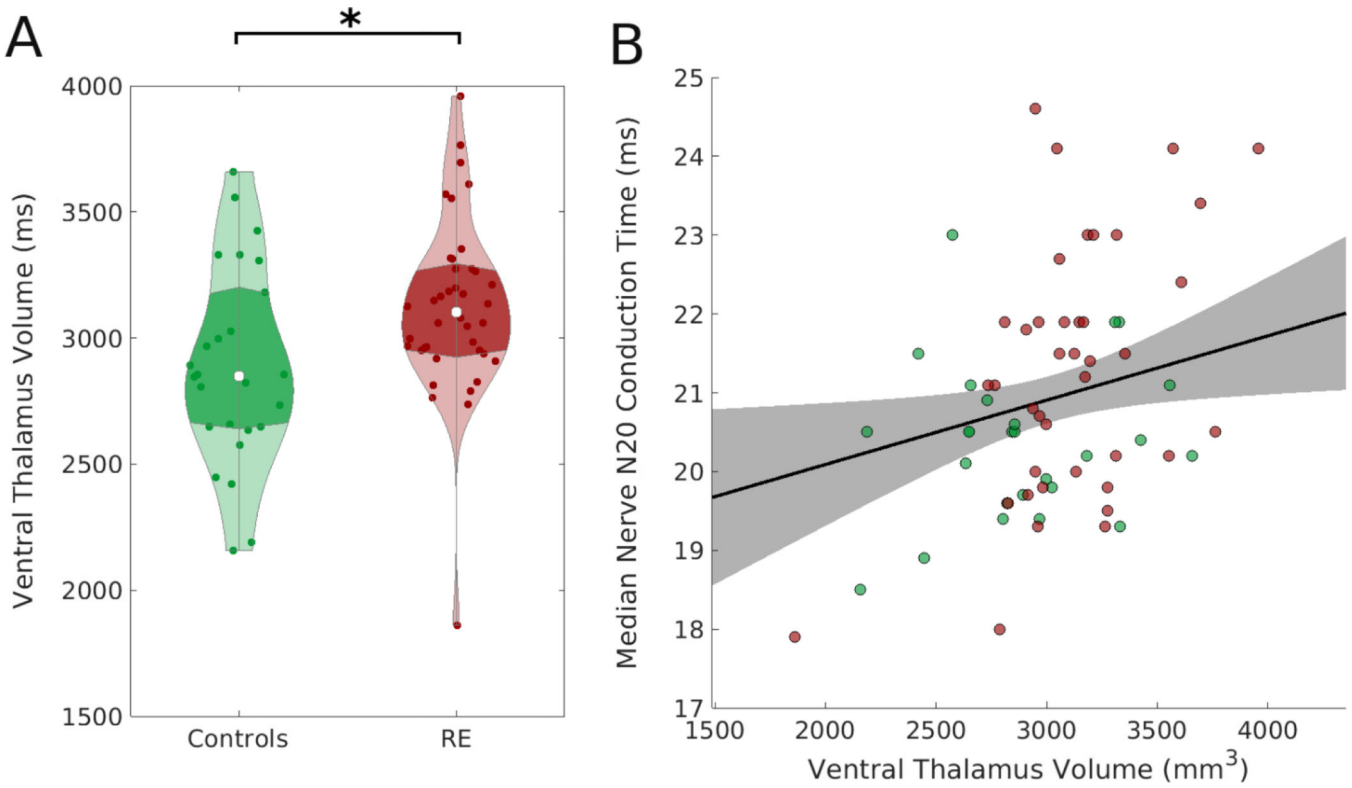

Figure 3. Ventral thalamic volume is larger in Rolandic epilepsy and positively correlates with Somatosensory Evoked Fields (SEF) conduction time.

A) Children with Rolandic Epilepsy (RE) have a larger ventral thalamic volume than controls (p=0.037). Violin plots (Bechtold, 2016) indicate the density of conduction time values, the violin width represents the number of points at each value, the white dot represents the median value, and the darker shading indicates the interquartile range. B) The ipsilateral ventral thalamic volume correlates with N20 median nerve conduction time (p=0.023). Points indicate individual subjects (green: controls, red: RE). The black line (shaded gray region) indicates linear mixed effects model fit (95% confidence interval).

Table 1.

Subject characteristics. RE: Rolandic Epilepsy; SEF: Somatosensory Evoked Fields; VEF: Visual Evoked Fields.

ID	Group	Age (years)	Sex	Duration Seizure Free (Months)	Anti-Seizure Medication	Centrotemporal Spikes	Experiment
1	RE	8.0	M	29	None	Left, Bilateral	SEF
2	RE	9.0	M	4	None	Right, Bilateral	SEF, VEF
3	RE	9.1	F	1	Keppra, Lamictal	Left, Bilateral	VEF
4	RE	9.1	M	0	None	None	SEF, SEF
5	RE	9.6	M	7	None	None	SEF, VEF
6	RE	9.8	M	0	Valproate; Vimpat	Right, Bilateral	SEF, VEF
7	RE	9.9	M	6	None	Right, Bilateral	SEF, VEF
8	RE	10.1	M	5	None	Not available	VEF
9	RE	10.4	M	26	Keppra	Right, Bilateral	SEF, VEF
10	RE	10.9	M	10	None	Left, Bilateral	SEF, VEF
11	RE	11.0	F	2	None	Left, Bilateral	SEF, VEF
12	RE	11.3	M	1	None	Right, Bilateral	VEF
13	RE	11.5	M	20	None	Left, Bilateral	SEF, VEF
14	RE	11.6	M	2	Keppra	None	SEF, VEF
15	RE	11.8	M	17	None	Left	SEF
16	RE	11.9	M	24	Keppra	Right, Bilateral	SEF, VEF
17	RE	12.8	M	18	Keppra	Right, Bilateral	SEF
18	RE	12.8	F	34	None	None	SEF, VEF
19	RE	13.3	M	26	Keppra	Left	SEF, VEF
20	RE	13.7	M	51	None	Right, Bilateral	SEF
21	RE	14.6	M	0	Onfi	Left	SEF, VEF
22	RE	14.7	M	0	Keppra	Left, Bilateral	SEF
23	RE	14.8	F	5	None	Right, Bilateral	VEF
24	RE	14.8	M	40	None	None	SEF, VEF
25	RE	14.9	M	38	None	Left	SEF, VEF

ID	Group	Age (years)	Sex	Duration Seizure Free (Months)	Anti-Seizure Medication	Centrotemporal Spikes	Experiment
26	RE	16.9	M	26	None	Left	SEF, VEF
27	Control	8.0	M				SEF
28	Control	8.7	M				SEF
29	Control	9.0	F				SEF, VEF
30	Control	9.4	F				SEF
31	Control	9.4	M				SEF
32	Control	10.5	F				SEF, VEF
33	Control	10.9	M				VEF
34	Control	11.5	M				VEF
35	Control	12.2	F				VEF
36	Control	12.9	F				VEF
37	Control	12.9	F				SEF, VEF
38	Control	13.4	F				VEF
39	Control	13.6	F				VEF
40	Control	14.0	F				SEF
41	Control	14.2	F				SEF, VEF
42	Control	14.3	M				SEF, VEF
43	Control	14.3	F				SEF, VEF
44	Control	14.4	M				SEF, VEF
45	Control	15.1	M				SEF, VEF

Table 2.

Diffusion MRIbased Connectivity Measurements. PCG: Postcentral gyrus.

Group	Connectivity Index
	Whole Thalamus to PCG – Left
RE	0.040 ± 0.016
Control	0.033 ± 0.016
	Whole Thalamus to PCG – Right
RE	0.042 ± 0.015
Control	0.024 ± 0.009
	Ventral Thalamus to PCG – Left
RE	0.035 ± 0.012
Control	0.040 ± 0.023
	Ventral Thalamus to PCG - Right
RE	0.037 ± 0.017
Control	0.028 ± 0.012